Bull. Chem. Soc. Ethiop. **2022**, 36(4), 843-858.
DOI: https://dx.doi.org/10.4314/bcse.v36i4.10
ISSN 1011-3924
Printed in Ethiopia
Online ISSN 1726-801X

SYNTHESIS, CHARACTERIZATION, BIOLOGICAL ACTIVITY, MOLECULAR DOCKING AND THERMAL ANALYSIS OF BINUCLEAR COMPLEXES

Khlood Abou-Melha*

Chemistry Department, Faculty of Science, King Khalid University, Abha, Saudi Arabia

(Received June 16, 2022; Revised June 19, 2022; Accepted June 20, 2022)

ABSTRACT. Because of their potential medical applications as antimicrobial medicines, metal-ligand complexes have sparked a lot of attention. Synthesis and characterization of various metal-diamine complexes were the goals of the research detailed in this paper. As a result, synthesis of new binuclear ligand; N,N'-bis(3-carboxysalcylidene)-4-chloro-1,2-phenylenediamine (H_4fsacph) which is derivative from the condensation of 3-formyl-2-hydroxybenzoic acid and 4-chlorobenzene-1,2-diamine has been performed. The new synthesized ligand has formed a mononuclear complex with Cu(II). The mononuclear Cu(II) complex was used to form binary nuclear complexes with some metal ions, like Cr(III), Mn(II), Fe(III), Ru(III), Pd(II) and La(III) ions. Elemental analysis, IR, UV-Visible, and thermal analyzes have been used to characterize the complexes. The interaction of a ligand with the receptors of *Candida albicans* and SARS-CoV-2 was predicted using molecular docking. Toward bacteria and fungi showing predominant activity against all fungi verified antibacterial activity of the synthesized complexes, while they have almost no activity against all bacteria. All compounds have shown antibacterial and antifungal activities, but the metal complexes showed better activities as compared to the original ligands, especially all zinc(II) complexes. The above results suggest that both ligands and their metal complexes have the potential to be explored as active pharmaceutical agents.

KEY WORDS: Molecular structure, Metal complexes, Molecular docking, Antimicrobial, SARS-CoV-2, Antifungal

INTRODUCTION

The presence of three extremely virulent coronaviruses that lead to human deadly pneumonia, namely SARS-CoV, SARS-CoV-2, and Middle East respiratory disease coronavirus, has thrown recent global events into disarray (MERS-CoV). The World Health Organization (WHO) announced on 30 January 2020 that the outbreak of COVID-19 is a worldwide healthiness concern [1, 2].

The World Health Organization in 2018 reported, 18.1 million new cases of cancer globally, with 9.6 deaths annually, with one in five men and one in six women expected to develop cancer in infancy, One out of every eight men and one out of every eleven women succumbs to the cancer. Female lung and breast cancers are the bulk of recent cases globally; Lung cancer (1.8 million fatalities, or 18.4% of all deaths), which has a bad prognosis, and colon cancer (881,000 deaths, or 9.2% of all deaths), stomach cancer (783,000 deaths), 8.2%, and hepatic cancer (881,000 deaths, 9.2%) handle the highest annual death rate (782,000 deaths, 8.2%). Schiff bases have sparked a considerable attention in recent years, and they've been used in a lot of different sectors. In latest days, Schiff bases have gained a lot of attention and have been used in a variety of industries [3, 4].

In recent years, Schiff bases have gained a lot of attention and have been used in a variety of industries [1, 2]. Although there are many different types of complexing and chelating ligands, Schiff bases are particularly interesting because of their vast range of uses in industrial and biology [3].

Because of their facile preparation and wide range of chelating potential of numerous metal ions, Schiff bases have been used successfully as ligands in coordination chemistry. Also, because

*Corresponding author. E-mail: Dr.khlood@hotmail.com

of their ease of synthesis and the wide range of chelating potential of many metal ions, Schiff bases have been used successfully as ligands in coordination chemistry. This is owing to their simplicity of synthesis, high solubility, structural variety, magnetic, spectroscopic, redox, and photocatalytic activity in common solvents. Because of their structural diversity and potential for a variety of applications, anticancer, anticonvulsant, antitumor, antifungal, antibacterial, anti-tuberculous, antioxidant, anti-carcinogenic action, antimalarial, anti-inflammatory, and DNA interaction and breakage are only a few of the applications for Schiff bases and their metal complexes. Sensors, solar cells, energy storage devices, and corrosion resistant methods can all benefit from them. The Schiff base complexes have been studied using electrochemical oxidation process, which are successful in electro catalysis and catalysis for a wide range of processes [5]. Scientists are focusing on the synthesis of new ligands capable of bringing two and/or three metal atoms into proximity through binuclear and tertiary nuclear complexes formation.

Werner was the first one to create binuclear complexes, noticing that complexes containing both platinum(II) and platinum(IV) have a darker color than their mononuclear counterparts [6, 7].

3-Formyl-2-hydroxybenzoic acid (H_2fsa) and amines or diamines are used to make Schiff bases were found as excellent binucleating ligands [7, 8]. This could act as a monobasic bidentate ligand or a dibasic bidentate ligand, depending on how its formyl and hydroxyl groups are used. It acts also acts as a bridging dibasic hexadentate ligand. Schiff bases of (H_2fsa) containing an alkyl or an aryl group monoamine can form binuclear chelates as shown in and mononuclear chelates. Schiff bases derived from (H_2fsa) and aliphatic or aromatic diamines can form mononuclear complexes with divalent metals [7, 9, 10].

The introduction of novel anti-microbial agents is the main goal of this investigation, together with antioxidants and anti-tumor/anticancer compounds to combat drug resistance and reduce issues related to negative effects of existing medications. For this purpose, a binuclear ligand has been synthesized from the reaction of the 3-formyl-2-hydroxybenzoic acid and 4-chlorobenzene-1,2-diamine. The new ligand N,N'-bis(3-carboxysalcylidene)-4-chloro-1,2-phenylenediamine was used to form a mononuclear complex with Cu(II). This mononuclear complex was used to for binuclear complexes with many metal ions. The new complexes were characterized by elemental analysis, IR, UV-Visible, magnetic studies, and thermal analyses. Antifungal and antibacterial experiments were carried out from a pharmacological standpoint.

EXPERIMENTAL

Materials

All the chemicals (E. Merck, Germany) were used without further purification. All metal chlorides used in our work, such as palladium(II) chloride $PdCl_2$ (M.Wt. = 177.3), ruthenium(III) chloride $RuCl_3$ (M.Wt. = 207.4), manganese(II) chloride tetrahydrate $MnCl_2.4H_2O$ (M.Wt. = 197.9), ferric chloride hexahydrate $FeCl_3.6H_2O$ (M.Wt. = 270.3), $CrCl_3.6H_2O$ (M.Wt. = 266.4), $CuCl_2.2H_2O$ (M.Wt. = 170.5), $NiCl_2.6H_2O$ (M.Wt. = 237.7), and $CoCl_2.6H_2O$ (M.Wt. = 237.9), were Merck (GR) grade. Lanthanum(III) chloride heptahydrate $LaCl_3.7H_2O$ (M.Wt. = 371.4) was BDH grade pure crystallized. Lithium hydroxide, $LiOH.H_2O$ (M.Wt. = 41.96) was obtained from Prolabo Company. They all were of extra pure reagent. All organic solvents extra pure grads were got from Prolabo and E. Merck companies. 4-Chlorobenzene-1,2-diamine was obtained from Fluka AG Company.

Preparation of the ligand and its complexes

The preparation of the ligand N,N'-bis(3-carboxysalicylidene)-4-chloro-1,2-phenylenediamine (H_4fsacph) and its complexes were discussed in details in the supporting information.

Antimicrobial studies

Tests for microbiological screening directly towards bacteria and fungi were carried out using fungi such as *Candida albicans*, *Aspergillus flavus*, and *Penicillium oxalicum*. While tested bacteria were *Escherichia coli* (Gram -ve bacteria), *Micrococcus luteus* (Gram +ve bacteria), and *Micrococcus roseus* (Gram +ve bacteria). Nutrient agar (N.A.) media mixed with one gram yeast per liter served as the culture medium. Antibacterial and antifungal activities of each complex were each sample was pre-incubated in 10 mL of Difco Nutrient Broth for 20 hours at 37 °C before being tested for bacteria using the traditional filter paper method. The agar medium employed in this investigation was made up of 3 g beef extract, 5 g peptone, and 15 g/L agar. Before sterilization, the medium was adjusted to a pH of 7 15 min at 121°C, kept in a 50 °C water bath. Each Petri plate received 20 mL of medium (10 mL diameter). Difco Nutrient Broth bacterial samples were diluted 5 times with sterilized physiological saline before being scattered on the agar plate using a sterile loop. After a 6-hour inoculation period (at room temperature), on the surface of the medium, discs carrying the various complexes were inserted. At a concentration of 0.5 mg/disc, the complexes were applied (Whatman No. 3 filter paper, 0.5 µm diameter). The plates were incubated at 37 °C for 24 hours to determine the zones of inhibition of microbial growth induced by the various complexes (mm). All the tests were done three times [11-14].

RESULTS AND DISSCUSION

The physical appearance, analytical data, and molecular weight of the Schiff base H_4fsacph and its mono copper complex Cu(H_2fsacph).2H_2O and binuclear copper complexes were determined and listed in Table 1 [15, 16].

Table 1. Some physical attributes and elemental analysis are dated to H_2fsacph, mono nuclear copper Cu(H_2fsacph).3H_2O and Cu(II) binuclear complexes.

No.	Compound	Color	Elemental analysis % Calc. (found)						Mwt. (g/mol)
			C	H	N	Cl	Cu	M"	
1	H_4fsacph	Yellow	60.02 (59.85)	3.42 (3.54)	6.38 (6.16)	8.09 (7.95)	-	-	438.5
2	Cu(H_2fsacph).3H_2O	Green	47.65 (47.65)	3.42 (3.51)	5.05 (5.09)	6.40 (6.20)	11.46 (11.20)	-	554.0
3	CuCr(fsacph)Cl.5H_2O	Green	39.08 (39.06)	3.10 (3.25)	4.14 (4.26)	10.51 (10.12)	9.40 (9.14)	7.68 (7.80)	675.5
4	CuMn(fsacph).3H_2O	Dark Brown	43.49 (43.79)	2.80 (2.84)	4.61 (5.09)	5.84 (4.96)	10.46 (9.88)	9.06 (8.94)	607
5	CuFe(fsacph)Cl.3H_2O	Deep Red	41.02 (40.79)	2.64 (2.61)	4.35 (4.13)	11.03 (10.95)	9.86 (9.53)	8.70 (8.70)	643.5
6	CuCo(fsacph).3.5H_2O	Deep Green	42.58 (43.00)	2.90 (2.65)	4.51 (4.80)	5.72 (4.98)	10.24 (10.07)	9.51 (9.19)	620
7	CuNi(fsacph).3H_2O	Deep Green	43.22 (43.02)	2.78 (2.79)	4.58 (4.55)	5.81 (5.00)	10.39 (9.40)	9.61 (9.32)	610.7
8	Cu_2(fsacph).3H_2O	Deep Green	40.52 (40.56)	3.13 (3.39)	4.29 (4.14)	5.44 (5.38)	19.49 (19.00)	-	651.5
9	CuRu(fsacph)Cl.6H_2O	Black	35.46 (35.48)	2.82 (2.89)	3.76 (3.78)	9.53 (9.27)	8.52 (8.46)	13.56 (12.87)	744.5
10	CuPd(fsacph).3H_2O	Black	40.09 (40.90)	2.27 (2.89)	4.25 (4.33)	5.39 (5.13)	9.64 (9.19)	16.16 (15.62)	658.4
11	CuLa(fsacph)Cl.4H_2O	Deep Green	35.46 (35.99)	2.55 (2.85)	3.76 (4.00)	9.53 (9.16)	8.53 (8.20)	18.66 (16.56)	744.4

IR spectra

To confirm the chemical structure of the prepared ligand N,N'-bis(3-carboxysalicylidene)-4-chloro-1,2-phenylenediamine (H_4fsacph) and its complexes, IR spectra were collected. The Infrared spectral data of the H_4fsacph, mono nuclear copper Cu(H_2fsacph).3H_2O and Cu(II) binuclear complexes are listed in Table 2. The infrared spectrum for the H_4fsacph ligand and mono Cu complex Cu(H_2fsacph).3H_2O exhibit weak bands appearing at 3040-3010 cm^{-1} and 2962-2853 cm^{-1} which can be attributed to the νC-H aromatic and of νC-H conjugated to the aromatic system, respectively. The free carboxylic groups of the free H_4fsacph and its Cu(H_2fsacph).3H_2O appeared at 1696 and 1681 cm^{-1}, respectively. The band appeared around 1582-1568 cm^{-1} in the copper binuclear complexes spectrum, can be attributed to the bonded carboxylate groups. The band at 1239 cm^{-1} at the spectrum of the free ligand H_4fsacph is tasked with the ν C-O phenolic stretching vibration. This band was red shifted to appear at range 1272-1258 cm^{-1} in the spectra of the complexes (**2-4**) representative that; oxygen atoms have been bonded with the metal ions. The phenolic group that acts as a link νC-O is appearing in the region 1580-1560 cm^{-1} as a shoulder that appear at 1527 cm^{-1} in a ligand that is free and at 1550 cm^{-1} when only one metal ion is connected (non-bridging), but in the present complexes this band could not be recognize owing to the strong absorption of the carboxylate groups νCOO^-. The band at 3400-3200 cm^{-1} when only one metal ion is connected (non-bridging). The band, which appears at 766-759 cm^{-1}, is assigned to tri-substitution of benzene rings; It can be found in the free ligand and copper mononuclear complex spectral Cu(H_2fsacph).3H_2O. The bands at 420-405 cm^{-1} can be credited to νCu-O bonds [17-19].

For the binuclear copper complexes, the aromatic νC-H Absorption in the area is usually caused by stretching vibrations 3075-3010 cm^{-1}. The νC-H the aromatic ring system's stretching vibration occurs at 2990 cm^{-1}. This mode of vibrations appears in the same region in the spectra of the Cu(II) binuclear complexes. The peak at 1629 cm^{-1} within the range of the free ligand as well as in the mononuclear spectrum complex Cu(H_2fsacph).3H_2O at 1614 cm^{-1} is given to the νC=N stretching vibration. This band is blue shifted to appear around 1616-1605 cm^{-1} in all Cu(II) binuclear complexes, indicating coordination with the ligand through the two nitrogen atoms of the azomethine groups [20]. The phenolic group that acts as a link νC-O is appearing in the region 1580-1560 cm^{-1} as a shoulder that appear around 1527 cm^{-1} in the free ligand while at 1550 cm^{-1} when a single metal ion is connected (non-bridging), but in the present complexes this band could not be recognize owing to the strong absorption of the carboxylate groups νCOO^-. The band located at 1239 cm^{-1} in the spectrum of the free ligand is to be allocated to νC-O phenolic stretching vibration, this band was red moved to appear at a range of 1268-1249 cm^{-1} in Cu(II) spectral properties binuclear complexes (**3-11**) indicating that; oxygen atoms have been bonded with the ions of metal. The existence of coordinated H_2O molecules in Cu(II) binuclear (**3-11**) complexes is evidenced based on the appearance of νHO band from the area 3412-3342 cm^{-1}. Band, which is present at 768-760 cm^{-1}, is assigned to tri-substitution at benzene rings. The bands located at 550-290 cm^{-1} may be ascribed to νM-N, νM-O and νM-Cl bonds. Table 2, Figure 1 and Figure 2 show infrared spectral data and plot of the H4fsacph, copper mononuclear complex Cu(H_2fsacph).3H_2O and copper binuclear complexes [21, 22].

Electronic spectra

The electronic absorption spectra of the free ligand N,N'-bis(3-carboxysalicylidene)-4-chloro-1,2-phenylenediamine H_4fsacph (**1**) and its mononuclear copper complex Cu(H_2fsacph).3H_2O (**2**) are recorded in the ultraviolet and visible region in the range 200-900 nm. The measured absorption spectral data are given in Table 3.

The spectrum of the free ligand N,N'-bis(3-carboxysalicylidene)-4-chloro-1,2-phenylenediamine H_4fsacph (**1**) represented four peaks at λ_{max}= 259, 308, 329 and 385 nm and a

shoulder appearing at 345 nm. The peak appearing at 259 nm is the appearance of absorption peaks transitions of type π-π*. The other three peaks can be ascribed to n-π* [23, 24].

Table 2. Infrared spectral data of the H_4fsacph, mono nuclear copper Cu(H_2fsacph).3H_2O and Cu(II) binuclear complexes.

Comp.	νOH	νC-O Phenol	νC-H Aromatic	νC-H Alkane	νtri-sub. of benzene	ν COOH	ν COO-	ν C=N	ν C-N	ν C-Cl	ν Cu-O	ν M"-O	ν M-N	ν M-Cl
H_4fsacph	3590sh, 1371s	1239 s	3019 w	2990w	759 sh	1696 s	-	1629 s		620 s	-	-	-	-
Cu(H_2fsacph).3H_2O	3454b, 1396s	1272 s	3010 w	2995w	2995 sh	1681s	-	-	1616 s	630 w	420 w	-	-	-
CuCr(fsacph)Cl.5H_2O	1399 s	1268 m	-	-	-	-	1580 s	-	1609 s	-	440 w	559 m	559 m	350 w
CuMn(fsacph).3H_2O	1384 s	1264 m	-	-	-	-	1576 s	-	1605 s	-	440 m	360 m	307 m	-
CuFe(fsacph)Cl.3H_2O	1386 s	1268 m	-	-	-	-	1580 s	-	1612 s	-	421 m	356 w	328 m	270 w
CuCo(fsacph).3.5H_2O	1391 s	1263 m	-	-	-	-	1579 s	-	1612 s	-	440 m	360 w	320 w	-
CuNi(fsacph).3H_2O	1395 s	1260 m	-	-	-	-	1580 s	-	1614 s	-	440 w	405 w	335 w	-
Cu_2(fsacph).3H_2O	1397 s	1263 m	-	-	-	-	1578 s	-	1607 s	-	423 m	423 w	494 w	-
CuRu(fsacph)Cl.6H_2O	1382 s	1275 m	-	-	-	-	1578 s	-	1606 s	-	440 m	360 w	460 w	300 w
CuPd(fsacph).3H_2O	1394 s	1269 m	-	-	-	-	1580 s	-	1613 s	-	430 m	390 w	470 w	-
CuLa(fsacph)Cl.4H_2O	1397 s	1266 m	-	-	-	-	1556 s	-	1609 s	-	440 w	520 w	405 w	300 w

s = strong; sh = sharp; b = broad; m = medium and w = weak.

The absorption spectra of the mononuclear copper complex Cu(H_2fsacph).3H_2O are not the same as the spectrum of the free ligand. The shoulder that developed at 345 nm and the two peaks that occurred at 329 and 385 nm vanished, and a new peak for copper appeared at 343 nm (H_2fsacph).3H_2O. The charge exchange between the ligand and the metal is responsible for this new peak. The absorption peak in the ultraviolet region due to intraligand transitions appearing at λ_{max}= 259 nm with molar absorptivity ε =1155 mol^{-1} cm^{-1} still visible in the spectra of mononuclear complex is the spectrum of the free ligand, but red shifted by 2.0 nm with increasing in molar absorptivity by 1030 mol^{-1} cm^{-1} for Cu(H_2fsacph).3H_2O. This is as a result of the combination of copper metal ions that formed. The alteration in the ligand's electronic conformation is what is responsible for the redshift and enhanced intensity of this band. The band due to intraligand charge transfer appearing at λ_{max}= 308 nm with molar absorptivity ε = 1575 mol^{-1} cm^{-1}. The peaks in the nujol mulls depict the complex of Cu's square planar structure (II) [25].

Generally, all Cu(II) binuclear complexes exhibited three strong peaks, the first peak appeared at 258–262 nm, that stands for intraligand π-π* transition [26]. The intraligand n-π* charge transfer was represented by the second peak, which emerged in the 306-309 nm region. L→Cu charge transfer is responsible for the third peak, which emerged in the region of 339.5-343.5 nm. The peaks, which appear at range 750-775 nm in nujol mull, can be attributed to d-d transition for square planar Cu(II) structure [27].

Table 3. The electronic absorption spectral data of the free ligand, mono nuclear copper $Cu(H_2fsacph).3H_2O$ and Cu(II) binuclear complexes, either in solution or as (nujol mulls).

Comp.	λ_{max} (nm)	ε (mol^{-1} cm^{-1})	Assignment
$H_4fsacph$	259	1155	π-π* trans.
	308	1575	n-π* trans.
	329	1276	n-π* trans.
	385	906	n-π* trans.
$Cu(H_2fsacph).3H_2O$	261	2185	π-π* trans.
	305	2390	n-π* trans.
	343	2130	L→Cu C.T.
	(750)	-	d-d trans.
$CuCr(fsacph)Cl.5H_2O$	261	2758	π-π* trans.
	306	2596	n-π* trans.
	343	2566	L→Cu C.T.
	(775)	-	d-d trans.
$CuMn(fsacph).3H_2O$	262	2761	π-π* trans.
	308	2695	n-π* trans.
	342	2780	L→Cu C.T.
	(775)	-	d-d trans.
$CuFe(fsacph)Cl.3H_2O$	261	2351	π-π* trans.
	306	2220	n-π* trans.
	339	2190	L→Cu C.T.
	(775)	-	d-d trans.
$CuCo(fsacph).3.5H_2O$	259	1736	π-π* trans.
	308	1605	n-π* trans.
	342	2032	L→Cu C.T.
	(750)	-	d-d trans.
$CuNi(fsacph).3H_2O$	260	2638	π-π* trans.
	307	2594	n-π* trans.
	342	2941	L→Cu C.T.
	(725)	-	d-d trans.
$Cu_2(fsacph).3H_2O$	259	2065	π-π* trans.
	309	1852	n-π* trans.
	340	2294	L→Cu C.T.
	(775)	-	d-d trans.
$CuRu(fsacph)Cl.6H_2O$	258	1838	π-π* trans.
	307	1618	n-π* trans.
	342	1888	L→Cu C.T.
	(775)	-	d-d trans.
$CuPd(fsacph).3H_2O$	258	1930	π-π* trans.
	307	1816	n-π* trans.
	342	1746	L→Cu C.T.
	(775)	-	d-d trans.
$CuLa(fsacph)Cl.4H_2O$	260	2247	π-π* trans.
	307	2287	n-π* trans.
	343	2708	L→Cu C.T.
	(775)	-	d-d trans.

Table 4 shows the magnetic moments of the mononuclear copper complex $Cu(H_2fsacph).3H_2O$ and Cu(II) binuclear complexes at T = 303 K. The measured μ_{eff} for the $Cu(H_2fsacph).3H_2O$ complex equal to 1.84 B.M. which is corresponds to experimental values of 1.85 B.M. resulted high spin Cu(II) complex with a square planar shape, by hyperdization of dsp^2 for Cu(II) complex [28, 29].

For Cu(II) binuclear complexes by comparing these values with the theoretical values calculated from the equation, $\mu_{eff} = \sqrt{(\mu_{Cu})^2 + (\mu_m)^2}$, we obtain the following results:

All of the Cu(II) ions that are located in the outer coordination site have been determined to have square planar configurations with dsp^2 hybrid. Square-planar divalent metal ions including Pd(II), Cu(II), Ni(II), Co(II), and Mn(II) are found inside the coordination site. La(III), Ru(III), Fe(III), and Cr(III) are examples of trivalent metal ions that are octahedral. The La(III) ion lacks an observable magnetic moment because the unpaired 4f electrons in La(III), which are known to be the cause of the paramagnetism, are relatively significantly screened from environmental influences by the overlaying and p electrons. This is consistent with the experimental value that was measured. Due to the antiferromagnetic spin exchange process involving Cu2+ and the other metal ions, the complexes **4**, **7**, and **8** have rather low magnetic moment values. But complexes **5**, **6**, **9**, **10** and **11** exhibit slightly larger magnetic moment values than that calculated, this is arising from the presence of ferromagnetic spin coupling interaction between Cu^{2+} and the metal ions. Complexes **4** and **5** with such Mn(II) and Fe(III) ions as their constituents have high magnetic moment values.

Table 4. The magnetic moment of the mono nuclear copper $Cu(H_2fsacph).3H_2O$ and Cu(II) binuclear complexes (**3-11**).

Comp.	μ_{eff} B.M. (found)	μ_{eff} B.M. (calc.)
$Cu(H_2fsacph).3H_2O$	1.84	1.85
$CuCr(fsacph)Cl.5H_2O$	4.20	4.14 – 4.24
$CuMn(fsacph).3H_2O$	5.94	6.21 – 6.25
$CuFe(fsacph)Cl.3H_2O$	6.45	6.10 – 6.13
$CuCo(fsacph).3.5H_2O$	4.74	3.23 – 3.29
$CuNi(fsacph).3H_2O$	4.21	4.25 – 4.30
$Cu_2(fsacph).3H_2O$	2.51	2.53 – 2.61
$CuRu(fsacph)Cl.6H_2O$	2.77	2.53 – 2.61
$CuPd(fsacph).3H_2O$	1.97	1.85 – 1.96
$CuLa(fsacph)Cl.4H_2O$	2.02	1.85 – 1.96

Thermal studies

Table 5 shows the thermal data for each step of the thermal decomposition of them. The TGA of free ligand N,N'-bis(3-carboxysalcylidene)-4-chloro-1,2-phenylenediamine show thermal stability up to 210 °C which indicates a lack of water molecules. Thermal breakdown takes place above this temperature. There are two fundamental processes; the first is the first step in the 210–350 °C temperature range and corresponds to the loss of two carboxylic groups, two phenolic groups, and an atom of chlorine. The reduction of all organic moieties, including three benzene rings and two azomethine groups, is taking place in the second stage, which is now occurring at 350–680 °C.

The loss of water lattice molecules, chlorine atoms, azomethine groups, benzene rings, oxygen atoms, hydroxyl groups, CO groups, CO_2, and the production of metal oxides are all part of the overall thermal disintegration process for complexes **2–11**. The process of fragmentation varies depending on the compound and the temperature.

Complexes **2** through **11** shed the water molecules in the 50–280 °C temperature range. For the other complexes, **3-6** and **8-10**, the loss of the chlorine ligand atom is a function of temperature 50-420 °C. Complexes **2**, **7**, and **11** lose the attached chlorine atom in the ligand between temperatures 50-280 °C. The metal bonded chlorine atoms are decomposed between temperatures 340–460 ºC for complexes **3**, **5** and **9**, while complex **10** decomposes in the temperature 250–500 ºC.

The loss of azomethine groups occurs in the temperature range 190-375 °C for complexes **2**, **3**, **6**, **8**, and **9**, in the temperature range 220-500 °C for complexes **7**, **10**, and **11**, and in the temperature range 390-460 °C for complexes **4** and **5**. In the temperature range of 180-660 °C, the loss of benzene rings occurs in two stages [23]. When the temperature drops below a certain threshold 250-700 °C for complexes **2–11**), CO_2 is released.

Table 5. Thermal data of the ligand, mono nuclear copper $Cu(H_2fsacph).3H_2O$ and Cu(II) binuclear complexes.

Compound	Step	T_i (ºC)	T_m (ºC)	T_f (ºC)	Weight loss %
$H_4fsacph$	1 st	210	290.81	350	35.5
	2 nd	350	470.86	680	64.2
$Cu(H_2fsacph).3H_2O$	1 st	50	152.58	380	16.6
	2 nd	280	369.64	370	23.1
	3 rd	370	383.10	390	39.5
	4 th	390	410.20	560	7.1
$CuCr(fsacph)Cl.5H_2O$	1 st	50	61.39	200	12.9
	2 nd	200	337.35	340	20.0
	3 rd	340	352.49	370	32.8
	4 th	370	482.06	620	6.3
$CuMn(fsacph).3H_2O$	1 st	50	65.92	180	9.2
	2 nd	180	358.70	400	18.0
	3 rd	400	439.47	450	9.1
	4 th	450	565.68	650	36.6
$CuFe(fsacph)Cl.3H_2O$	1 st	50	77.70	220	7.9
	2 nd	220	368.80	390	17.6
	3 rd	390	420.97	460	29.8
	4 th	460	484.91	630	15.6
$CuCo(fsacph).3.5H_2O$	1 st	50	70.65	190	9.8
	2 nd	190	355.50	360	25.7
	3 rd	360	398.78	410	13.9
	4 th	410	422.34	430	7.5
	5 th	430	455.99	590	16.5
$CuNi(fsacph).3H_2O$	1 st	50	65.57	250	13.2
	2 nd	250	385.28	425	25.4
	3 rd	425	551.87	660	36.3
$Cu_2(fsacph).3H_2O$	1 st	50	60.39	160	8.6
	2 nd	160	244.71	275	5.7
	3 rd	275	338.58	360	20.0
	4 th	360	401.73	410	13.4
	5 th	410	434.16	580	15.8
	6 th	580	695.29	700	6.5
$CuRu(fsacph)Cl.6H_2O$	1 st	50	67.32	170	14.4
	2 nd	170	353.38	375	18.1
	3 rd	375	398.81	400	9.7
	4 th	400	413.96	425	23.0
	5 th	425	454.34	560	5.6
$CuPd(fsacph).3H_2O$	1 st	50	53.49	220	8.1
	2 nd	220	376.57	420	54.9
	3 rd	420	534.74	640	6.4
$CuLa(fsacph)Cl.4H_2O$	1 st	50	64.06	250	13.7
	2 nd	250	355.17	500	52.6

T_i = Initial temperature, T_m = Peak temperature and T_f = Final temperature.

Conductometric studies

Using DMSO as the solvent, the conductance measurements were performed on 1.0 x 10^{-3} M of the produced complexes (**2–11**). The corresponding data is listed in Table 6. Due to their nonelectrolytic (non-ionic) characteristics, these complexes have low molar conductance values [31, 32].

Table 6. The molar conductivity data of the mono nuclear copper $Cu(H_2fsacph).3H_2O$ and Cu(II) binuclear complexes (**2-11**).

Complex	S cm^2 mol^{-1}
$Cu(H_2fsacph).3H_2O$	16
$CuCr(fsacph)Cl.5H_2O$	18
$CuMn(fsacph).3H_2O$	29
$CuFe(fsacph)Cl.3H_2O$	11
$CuCo(fsacph).3.5H_2O$	21
$CuNi(fsacph).3H_2O$	20
$Cu_2(fsacph).3H_2O$	28
$CuRu(fsacph)Cl.6H_2O$	11
$CuPd(fsacph).3H_2O$	18
$CuLa(fsacph)Cl.4H_2O$	18

Molecular docking

Anticovid-19

By using MOE.2015.10 software, we can operate the molecular docking calculation. The key SARS-CoV-2 protease was found in the database of proteins (PDB ID: 6YB7, chain A). Following the model's verification, coordinated protein sequences. Following that, molecular docking was utilized to evaluate the antiviral activity of the formerly described medications, and SARS-CoV-2 protease from natural origin. In each case, the constants of energy and inhibition are given all of the chemicals were optimized in their active physiological settings. Before ensuring that the evaluated medicines and the ligand N,N'-bis(3-carboxysalcylidene)-4-chloro-1,2-phenylenediamine ($H_4fsacph$) were in the optimal active state. SARS-CoV-2 protease $H_4fsacph$ was screened against. Last, the ligands used were chosen based on studies of the expected modes of binding and their ratings [33-36].

Lower docking molecular scores indicate that compounds have a stronger affinity for the 6YB7 protein. The direction of a ligand is determined using a form scoring characteristic that estimates the energies of the ligand-binding receptor. The analytical value of form scoring is related to van der van der Waals' appealing power. Energy minimizing once the initial orientation has been completed, as well as score reviews to identify the closest energy evaluation within the receptor-binding locations, minimization sites. Since then, the complex produced between the ligands screened with greater binding energies has been extremely stable, and SARS-primary CoV-2's protease has been identified. The ligand's capacity to bind the receptors that bind to the virus is revealed by the formation of inappropriate hydrogen bonding with the main protease chain. The docking value was -6.7, and the binding involving $H_4fsacph$ and 6YB7 by one hydrogen bond with Arg 4 is shown in Table 7.

Anti-candida albicans

In this analysis, *Candida albicans*' primary protease was removed from the protein database (1zap). While *Candida* was found in the protein database (1ZAP). Binding energies are the most

common way of determining a ligand's binding [37]. Therefore, the ligand's binding affinity to the receptor would be increased due to a decrease in binding energy resulting from mutations [38]. The existence of multiple open active hydrogen bonding sites is a distinguishing feature of ligands. This property allows them to be effective protein binders and aids in the production of inhibitory chemicals. Results specify that a successful *Candida albicans* mutant 1ZAP-Hormone inhibitor. The docking value was -6.56, and the interaction of H_4fsacph and H_4fsacph was revealed in Table 7 and 1ZAP by one hydrogen bond with ASP 32 and one π–π interaction with Ser 35.

Table 7. Molecular docking mode and interaction for the N,N'-bis(3-carboxysalcylidene)-4-chloro-1,2-phenylenediamine (H_4fsacph) H_4fsacph ligand.

Protein	2D	3D	Inter-pretation	Docking score
SARS-CoV-2 protease (ID : 6YB7)	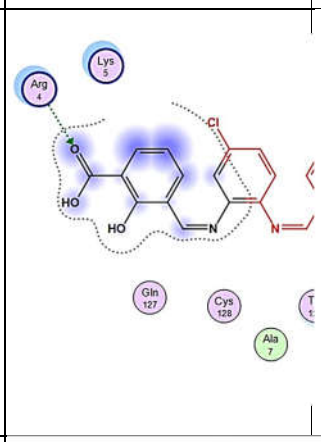	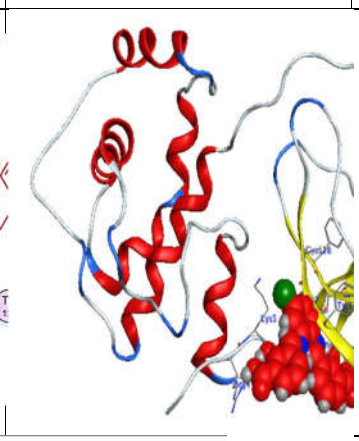	One π–π interaction with Arg 4	-6.7
Candida albicans (ID: 1zap)	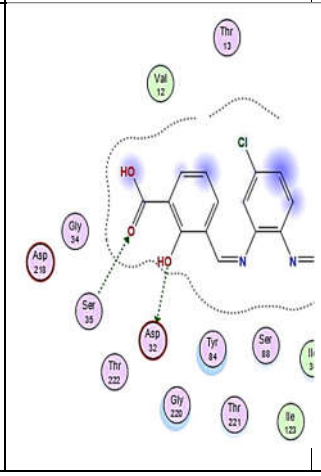	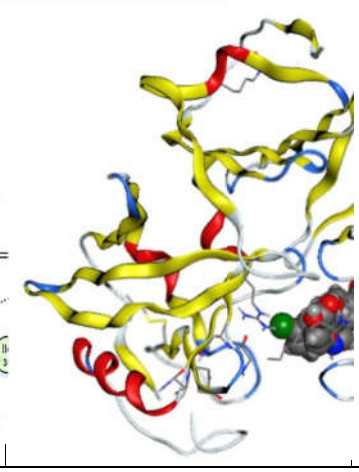	One π–π interaction with Ser 35 And one Hydrogen bond with ASP 32	-6.56

Molecular structure

The 3-21G base set of the HF method has optimized the molecular structure of the N,N'-bis(3-carboxysalcylidene)-4-chloro-1,2-phenylenediamine (H_4fsacph). Using the programmed Gauss View was used to create the molecule and optimized [39].

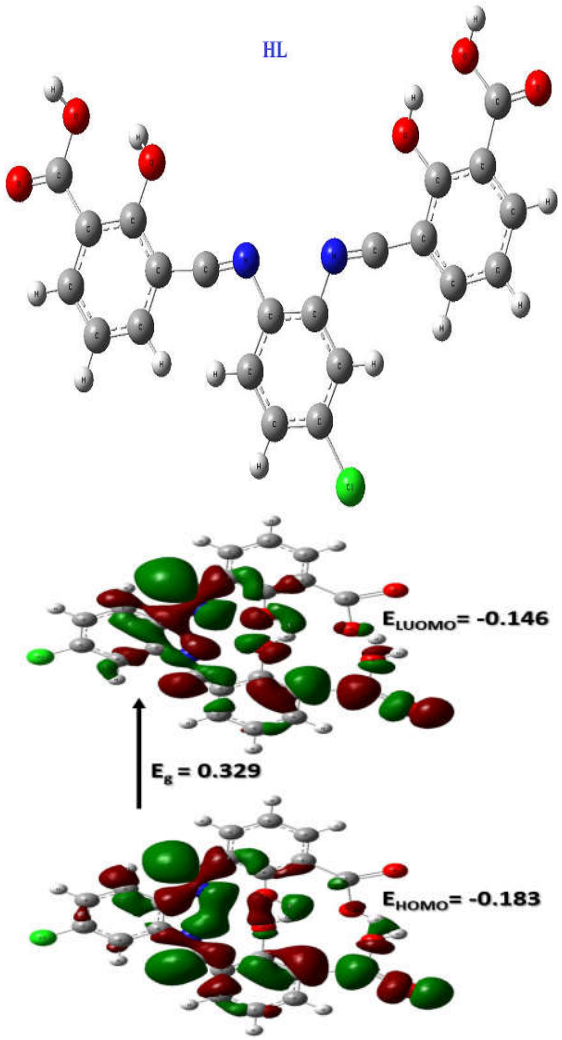

Figure 1. (a) Optimized structure of H_4fsacph. (b) HOMO and LUMO using the B3LYP.

Table 8. Quantum chemical parameters calculated for the H_4fsacph under investigation.

Compound	E_{HUMO} eV	E_{LUMO} eV	ΔE eV	X eV	η eV	Pi eV	σ eV	S eV	Ω eV	ΔN_{max}
H_4fsacph	-0.183	-0.146	0.04	0.16	0.2	-0.16	6.07	0.01	-8.89	8.89

The crucial traits are HOMO and LUMO, which are frequently used to chemically characterise the responsiveness of a system. EHOMO, ELUMO, and Egap of H_4fsacph are shown in Figure 1. Table 8 represented the E_{HOMO}, E_{LUMO}, and E_{gap} of H_4fsacph. In fact, theoretically, the E_{gap} is a

crucial indicator of the chemical acuteness of a ligand, with a small gap signifying strong chemical reactivity (low steady) and a large gap signifying reduced chemical reactivity (high stable) (highly steady).

The theoretical elements, HOMO (π-donor) and LUMO (π-acceptor), are crucial to the architecture of molecules. The E_{HOMO} and E_{LUMO} principles, EHOMO–LUMO is distinguished from all other compounds by its energy difference Table 8. It is possible to assess the stability of molecules and the softness of compounds using the difference in energy. The molecule's lesser polarizability results from its lower energy volume (more reactive) [40].

Electron Density Molecular Electrostatic Potential (MEP)

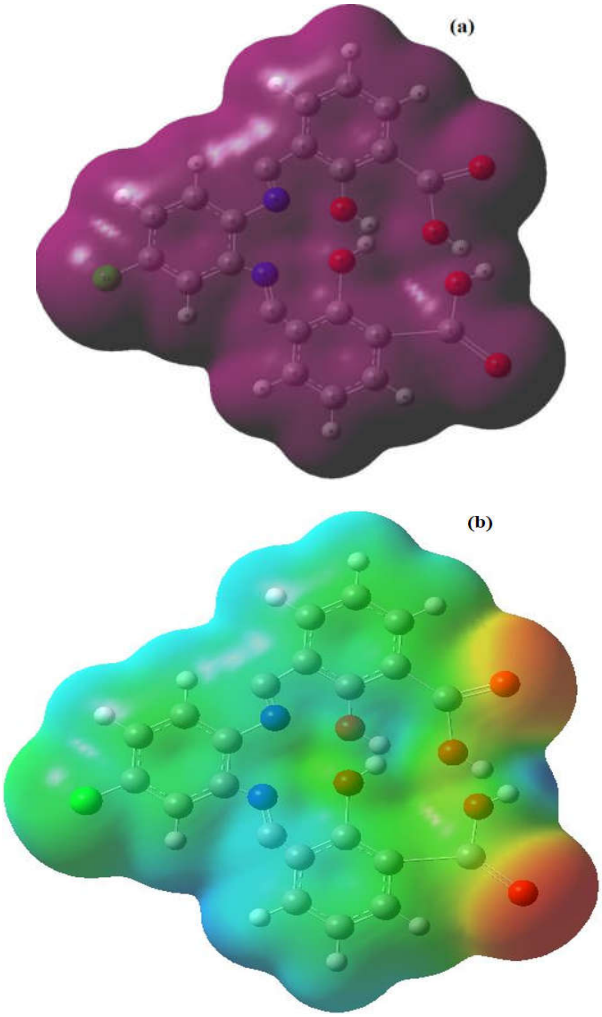

Figure 2. The N,N'-bis(3-carboxysalcylidene)-4-chloro-1,2-phenylenediamine H_4fsacph was utilized to map the whole electron density surface using molecular electrostatic potential (MEP).

Active sites

A technique for assessing the reactive groups in the evaluated adsorbate/adsorbents system and understanding the areas of electrophilic/nucleophilic attack and electrostatic potential zero regions is molecular electrostatic potential (MEP). Utilizing molecular electrostatic potentials (MEP), the whole N,N'-bis(3-carboxysalcylidene)-4-chloro-1,2-phenylenediamine (H_4fsacph) electron density region was found in this work (Figure 2). The different values of the MEP were shown on these maps using a range of colors (blue, light blue, green, yellow, and red). Likewise, the negative values of the MEP were represented by red and yellow colors, which are associated with electrophilic assault; the qualities were represented by blue colors, which are associated with nucleophilic attack; and the MEP zero area was represented by green [41].

Microbiological screening

Using fungi like *Aspergillus flavus*, *Candida albicans*, and *Penicillium oxalicum*, tests for microbiological screening directly towards bacteria and fungi were conducted. *Escherichia coli* (Gram -ve bacteria), *Micrococcus luteus* (Gram +ve bacteria), and *Micrococcus roseus* (Gram +ve bacteria) were the tested bacteria. Nutrient agar (N.A.) media supplemented with one gram of yeast per liter served as the culture medium. Each complex's antibacterial and antifungal properties were assessed using the traditional filter paper method previously described [37, 42]. The produced complexes (**1–11**) clearly display dominating activity against all fungi, but essentially negligible activity against all bacteria [38].

CONCLUSION

The production of the new ligand (H4fsacph) and its mono- and binuclear complexes are discussed in this paper. The composition of the produced compounds and their activity were confirmed using characterization techniques and biological activities. These compounds are stable according to spectroscopic, magnetic, thermal, theoretical data, and the low energies of the HOMO and LUMO orbitals in the IR spectrum. The thermogravimetric study of the complexes reveals that the breakdown processes involve more than two phases. By attaching to the primary protease of SARS-CoV-2, H4fsacph was employed in molecular docking to evaluate its activity against COVID-19, which has antifungal properties with the *Candida albicans* 1zap receptor and was retrieved from the RCSB protein data library using PDB (ID: 6YB7).

REFERENCES

1. Bogoch, I.I.; Watts, A.; Thomas-Bachli, A.; Huber, C.; Kraemer, M.U.; Khan, K. Pneumonia of unknown aetiology in Wuhan, China: potential for international spread via commercial air travel. *J. Travel. Med.* **2020**, 27, taaa008. DOI: 10.1093/jtm/taaa008.
2. El-Bindary, A.A.; Toson, E.A.; Shoueir, K.R.; Aljohani, H.A.; Abo-Ser, M.M.; Metal–organic frameworks as efficient materials for drug delivery: Synthesis, characterization, antioxidant, anticancer, antibacterial and molecular docking investigation. *Appl. Organomet. Chem.* **2020**, 34, e5905.
3. Wu, C.; Liu, Y.; Yang, Y.; Zhang, P.; Zhong, W.; Wang, Y.; Wang, Q.; Xu, Y.; Li, M.; Li, X. Analysis of therapeutic targets for SARS-CoV-2 and discovery of potential drugs by computational methods. *Acta Pharm. Sin. B.* **2020**, 10, 766-788.
4. Awual, M.R.; Yaita, T.; El-Safty, S.A.; Shiwaku, H.; Suzuki, S.; Okamoto, Y. Copper(II) ions capturing from water using ligand modified a new type mesoporous adsorbent. *Chem. Eng. J.* **2013**, 221, 322-330.

5. El-Bindary, A.A.; El-Sonbati, A.; El-Mosalamy, E.; Ahmed, R. Potentiometric and thermodynamic studies of azosulfonamide drugs. *Chem. Pap.* **2003**, 57, 255.
6. Fizer, M.; Sidey, V.; Tupys, A.; Ostapiuk, Y.; Tymoshuk, O.; Bazel, Y. On the structure of transition metals complexes with the new tridentate dye of thiazole series: Theoretical and experimental studies. *J. Mol. Struct.* **2017**, 1149, 669-682.
7. Zhu, N.; Zhang, D.; Wang, W.; Li, X.; Yang, B.; Song, J.; Zhao, X.; Huang, B.; Shi, W.; Lu, R. A novel coronavirus from patients with pneumonia in China, 2019. *N. Engl. J. Med.* **2020**, 382, 727-733.
8. Joshi, H.; Singh, B.; Saxena, G.K.; Singh, V.; Singh, R.P.; Arya, E. Synthesis and characterization of novel halogens substituted coumarin-aldehyde. *Int. J. Chem. Pharm. Sci.* **2012**, 4,19-23.
9. Weigt, S.; Huebler, N.; Strecker, R.; Braunbeck, T.; Broschard, T.H. Developmental effects of coumarin and the anticoagulant coumarin derivative warfarin on zebrafish (Danio rerio) embryos. *Reprod. Toxicol.* **2012**, 33, 133-141.
10. Xia, S.; Liu, M.; Wang, C.; Xu, W.; Lan, Q.; Feng, S.; Qi, F.; Bao, L.; Du, L.; Liu, S. Inhibition of SARS-CoV-2 (previously 2019-nCoV) infection by a highly potent pan-coronavirus fusion inhibitor targeting its spike protein that harbors a high capacity to mediate membrane fusion. *Cell Res.* **2020**, 30, 343-355.
11. Wolfe, A.; Shimer, Jr. G.H.; Meehan, T. Polycyclic aromatic hydrocarbons physically intercalate into duplex regions of denatured DNA. *Biochemistry* **1987**, 26, 6392-6396.
12. Reichmann, M.; Rice, S.; Thomas, C.; Doty, P.A. Further examination of the molecular weight and size of desoxypentose nucleic acid. *J. Am. Chem. Soc.* **1954**, 76, 3047-3053.
13. Shoair, A.; El-Shobaky, A.; Azab, E. Synthesis, characterization, DNA binding and catalytic applications of Ru(III) complexes. *Spectrochim. Acta Part A* **2015**, 151, 322-334.
14. El-Safty, S.A.; Shahat, A.; Mahmoud, M.M; Nguyen, H.; Warkocki, W.; Ohnuma, M. Mesoporous silica nanotubes hybrid membranes for functional nanofiltration. *Nanotechnology* **2010**, 21, 375603.
15. Mohamed, G.; Hassan, N.; Shahat, A.; El-Didamony, A.; Ashraf, A. Synthesis and characterization of porous magnetite nanosphere iron oxide as a novel adsorbent of anionic dyes removal from aqueous solution. *Biointerface Res. Appl. Chem.* **2021**, 11, 13377-13401.
16. Awual, M.R.; Hasan, M.M.; Khaleque, M.A.; Sheikh, M.C. Treatment of copper(II) containing wastewater by a newly developed ligand based facial conjugate materials. *Chem. Eng. J.* **2016**, 288, 368-376.
17. Satyanarayana, S.; Dabrowiak, J.C.; Chaires, J.B. Tris (phenanthroline) ruthenium(II) enantiomer interactions with DNA: Mode and specificity of binding. *Biochemistry* **1993**, 32, 2573-2584.
18. Shahat, A.; Elsalam, S.A.; Herrero-Martínez, J.M.; Simó-Alfonso, E.F.; Ramis-Ramos, G. Optical recognition and removal of Hg(II) using a new self-chemosensor based on a modified amino-functionalized Al-MOF. *Sens. Actuators B* **2017**, 253, 164-172
19. El-Bindary, A.A.; El-Sonbati, A.Z.; Kera, H.M. Thermodynamics of substituted pyrazolone. V: Potentiometric and conductometric studies of complexes of some transition metals with 4-(4-acetophenyl) hydrazono-3-methyl-2-pyrazolin-5-one. *Can. J. Chem.* **1999**, 77, 1305-1309.
20. Diab, M.; El-Sonbati, A.; El-Bindary, A.; Barakat, A. Supramolecular spectral studies on metal–ligand bonding of novel quinoline azodyes. *Spectrochim. Acta Part A* **2013**, 116, 428-439.
21. Guo, Hx.; Wang, F.; Yu, Kq.; Chen, J.; Bai, D.; Chen, K.; Shen, X.; Jiang, H. Novel cyclophilin D inhibitors derived from quinoxaline exhibit highly inhibitory activity against rat mitochondrial swelling and Ca^{2+} uptake/release. *Acta Pharmacol. Sin.* **2005**, 26, 1201-1211.
22. Shahat, A., Trupp, S. Sensitive, selective, and rapid method for optical recognition of ultra-traces level of Hg(II), Ag(I), Au(III), and Pd(II) in electronic wastes. *Sens. Actuators B* **2017**, 245, 789-802.

23. Hassan, N.; El-Sonbati, A.; El-Desouky, M. Synthesis, characterization, molecular docking and DNA binding studies of Cu(II), Ni(II), Zn(II) and Mn(II) complexes. *J. Mol. Liq.* **2017**, 242, 293-307.
24. Awual, M.R.; Rahman, I.M.; Yaita, T.; Khaleque, M.A.; Ferdows, M. pH dependent Cu(II) and Pd(II) ions detection and removal from aqueous media by an efficient mesoporous adsorbent. *Chem. Eng. J.* **2014**, 236, 100-109.
25. El-Sonbati, A.; Diab, M.; El-Bindary, A.; Abou-Dobara, M.; Seyam, H. Supramolecular coordination and antimicrobial activities of constructed mixed ligand complexes. *Spectrochim. Acta Part A* **2013**, 104, 213-221.
26. Chio, C.H.; Sharma, S.K.; Muenow, D.W. The hydrates and deuterates of ferrous sulfate ($FeSO_4$): A Raman spectroscopic study. *J. Raman Spectrosc.* **2007**, 38, 87-99.
27. Shahat, A.; Mohamed, M.H.; Awual, M.R.; Mohamed, S.K. Novel and potential chemical sensors for Au(III) ion detection and recovery in electric waste samples. *Microchem. J.* **2020**, 158, 105312.
28. Bharti, A.C;. Vishnoi, K.; Singh, S.M.; Aggarwal, B.B. *Pathways, Linked to Cancer Chemoresistance and Their Targeting by nutraceuticals. Role of Nutraceuticals in Cancer Chemosensitization*, Elsevier: Amsterdam; **2018**; pp. 1-30.
29. El-Safty, S.A.; Shahat, A.; Ismael, M. Mesoporous aluminosilica monoliths for the adsorptive removal of small organic pollutants. *J. Hazard. Mater.* **2012**, 201-202, 23–32.
30. Chitrala, K.N.; Yang, X.; Busbee, B.; Singh, N.; Bonati, L.; Xing, Y.; Nagarkatti, P.; Nagarkatti, M. Computational prediction and in vitro validation of VEGFR1 as a novel protein target for 2,3,7,8-tetrachlorodibenzo-*p*-dioxin. *Sci. Rep.* **2019**, 9, 1-12.
31. El-Ghamaz, N.; El-Sonbati, A.; Diab, M.; El-Bindary, A.; Awad, M.; Morgan, S.M. Dielectrical, conduction mechanism and thermal properties of rhodanine azodyes. *Mater. Sci. Semicond. Process* **2014**, 19, 150-162.
32. Diab, M.; El-Bindary, A.; El-Sonbati, A.; Salem, O. Supramolecular structure and substituents effect on the spectral studies of dioxouranium(VI) azodyes complexes. *J. Mol. Struct.* **2012**, 1007, 11-19.
33. El-Sonbati. A.; Diab, M.; El-Halawany, M.; Salam, N. Polymer complexes: XLXII-interplay of coordination π–π stacking and hydrogen bonding in supramolecular assembly of [sulpha drug derivatives-N,S:N,O] complexes. *Spectrochim. Acta Part A* **2010**, 77, 755-766.
34. Coats, A.W.; Redfern, J. Kinetic parameters from thermogravimetric data. *Nature* **1964**, 201, 68-69.
35. Horowitz, H.H.; Metzger G. A new analysis of thermogravimetric traces. *J. Anal. Chem.* **1963**, 35, 1464-1468.
36. El-Bindary, A.; Hassan, N.; El-Afify, M. Synthesis and structural characterization of some divalent metal complexes: DNA binding and antitumor activity. *J. Mol. Liq.* **2017**, 242, 213-228.
37. Huang, C.; Wang, Y.; Li, X.; Ren, L.; Zhao, J.; Hu, Y.; Zhang, L.; Fan, G.; Xu, J.; Gu X. Clinical features of patients infected with 2019 novel coronavirus in Wuhan, China. *J.-Lancet.* **2020**, 395, 497-506.
38. Gautret, P.; Lagier, J.C.; Parola, P.; Meddeb, L.; Mailhe, M.; Doudier, B.; Courjon, J.; Giordanengo, V.; Vieira, V.; Dupont, H. Hydroxychloroquine and azithromycin as a treatment of COVID-19: Results of an open-label non-randomized clinical trial. *Int. J. Antimicrob. Agents* **2020**, 105949. DOI: 10.1016/j.ijantimicag.2020.105949.
39. Hassan, N.; El-Sonbati, A.Z.; El-Desouky, M.G. Synthesis, characterization, molecular docking and DNA binding studies of Cu(II), Ni(II), Zn(II) and Mn(II) complexes. *J. Mol. Liq.* **2017**, 242, 293-307.
40. El-Bindary, M.; El-Desouky, M.; El-Bindary, A. Adsorption of industrial dye from aqueous solutions onto thermally treated green adsorbent: A complete batch system evaluation. *J. Mol. Liq.* **2021**, 117082. DOI: 10.1016/j.molliq.2021.117082.

41. Nakhli, A.; Bergaoui, M.; Toumi, K.H.; Khalfaoui, M.; Benguerba, Y.; Balsamo, M.; Soetaredjo, F.; Ismadji, S.; Ernst, B.; Erto, A. Molecular insights through computational modeling of methylene blue adsorption onto low-cost adsorbents derived from natural materials: A multi-model's approach. *Computers Chem. Eng.* **2020**, 140, 106965.
42. Kalaivanan, C.; Sankarganesh, M.; Suvaikin, M.Y.; Karthi, G.B.; Gurusamy, S.; Subramanian, R.; Asha, R.N. Novel Cu(II) and Ni(II) complexes of nicotinamide based Mannich base: Synthesis, characterization, DFT calculation, DNA binding, molecular docking, antioxidant, antimicrobial activities. *J. Mol. Liq.* **2020**, 320, 114423.